Science Signaling
AAAS

www.sciencesignaling.org/cgi/content/full/8/395/ra95/DC1

Supplementary Materials for

Dichotomous roles for externalized cardiolipin in extracellular signaling: Promotion of phagocytosis and attenuation of innate immunity

Krishnakumar Balasubramanian,* Akihiro Maeda, Janet S. Lee, Dariush Mohammadyani, Haider Hussain Dar, Jian Fei Jiang, Claudette M. St. Croix, Simon Watkins, Vladimir A. Tyurin, Yulia Y. Tyurina, Katharina Klöditz, Anastassia Polimova, Valentyna I. Kapralova, Zeyu Xiong, Prabir Ray, Judith Klein-Seetharaman, Rama K. Mallampalli, Hülya Bayir, Bengt Fadeel,* Valerian E. Kagan*

*Corresponding author. E-mail: kris.balasub@gmail.com (K.B.); bengt.fadeel@ki.se (B.F.); kagan@pitt.edu (V.E.K.)

Published 22 September 2015, *Sci. Signal.* **8**, ra95 (2015)
DOI: 10.1126/scisignal.aaa6179

The PDF file includes:

Fig. S13. CL does not inhibit the flagellin-stimulated secretion of cytokines.
Fig. S14. Predicted binding poses of lipid A, TLCL, and lipid IVA to the TLR4-MD2 complex as determined by molecular docking simulations.
Table S1. The binding energies of lipid A, TLCL, and *E. coli* CLs with MD2.

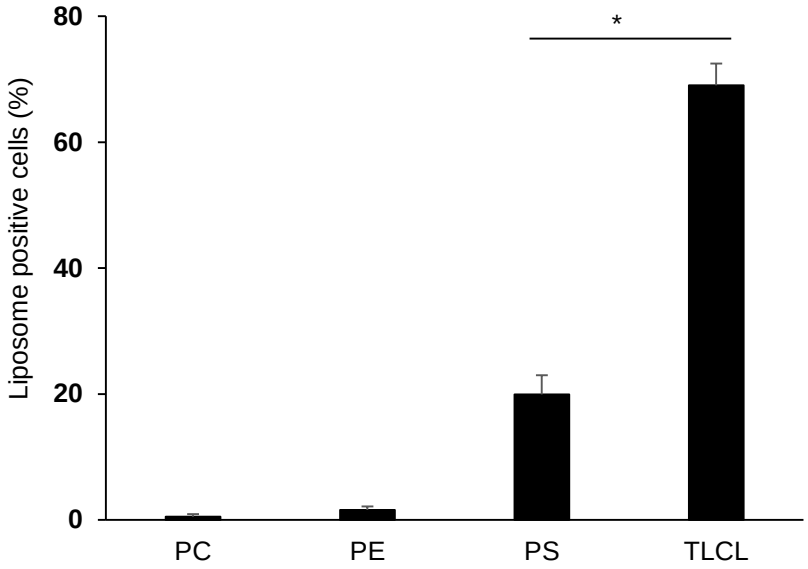

Fig. S1. Comparison of PS- and TLCL-dependent phagocytosis by RAW 264.7 cells. RAW 264.7 cells were incubated for 60 min with fluorescent liposomes composed of the indicated phospholipids (7 nmol) in PC. The cells were then washed, trypsinized, and assessed for phagocytosis by flow cytometric analysis as described earlier. Data are means ± SD of three experiments. **P* < 0.01 by t-test.

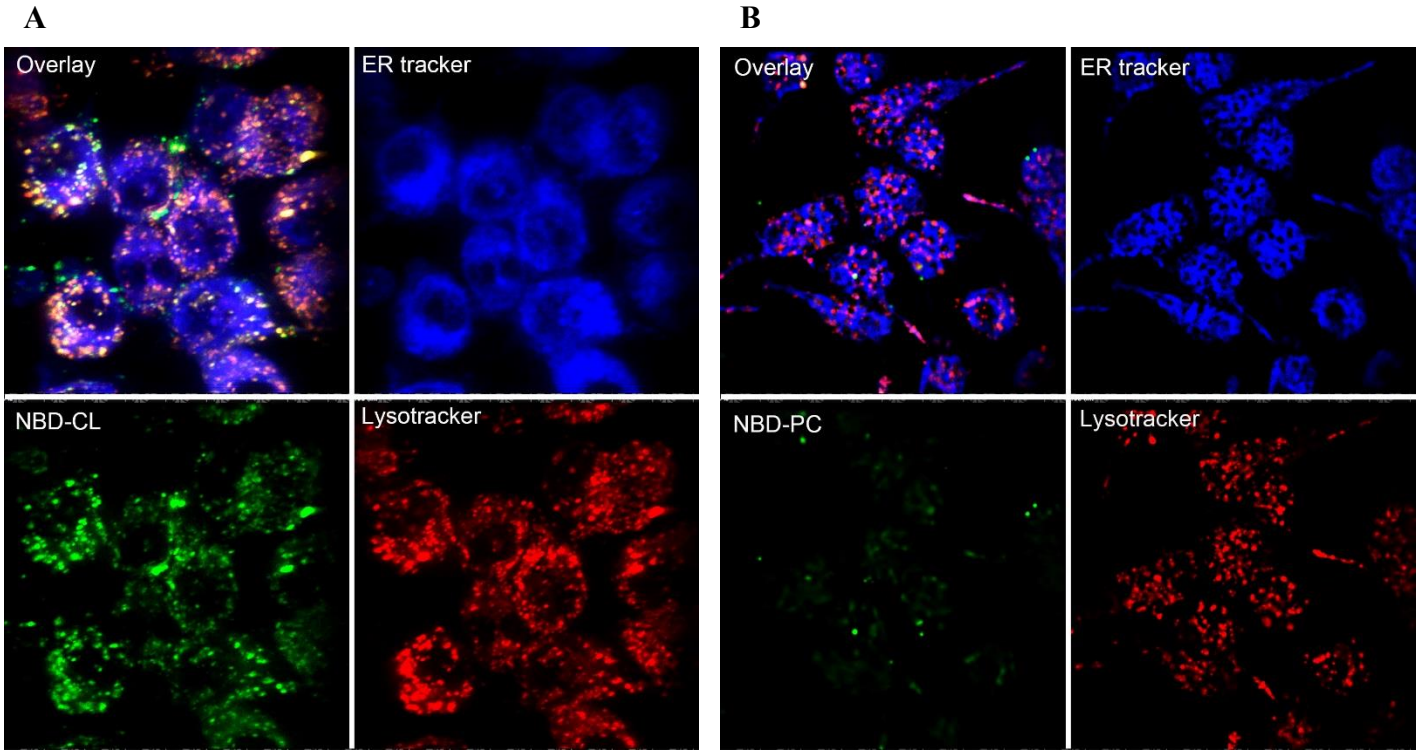
A
Overlay
ER tracker
NBD-CL
Lysotracker
B
Overlay
ER tracker
NBD-PC
Lysotracker

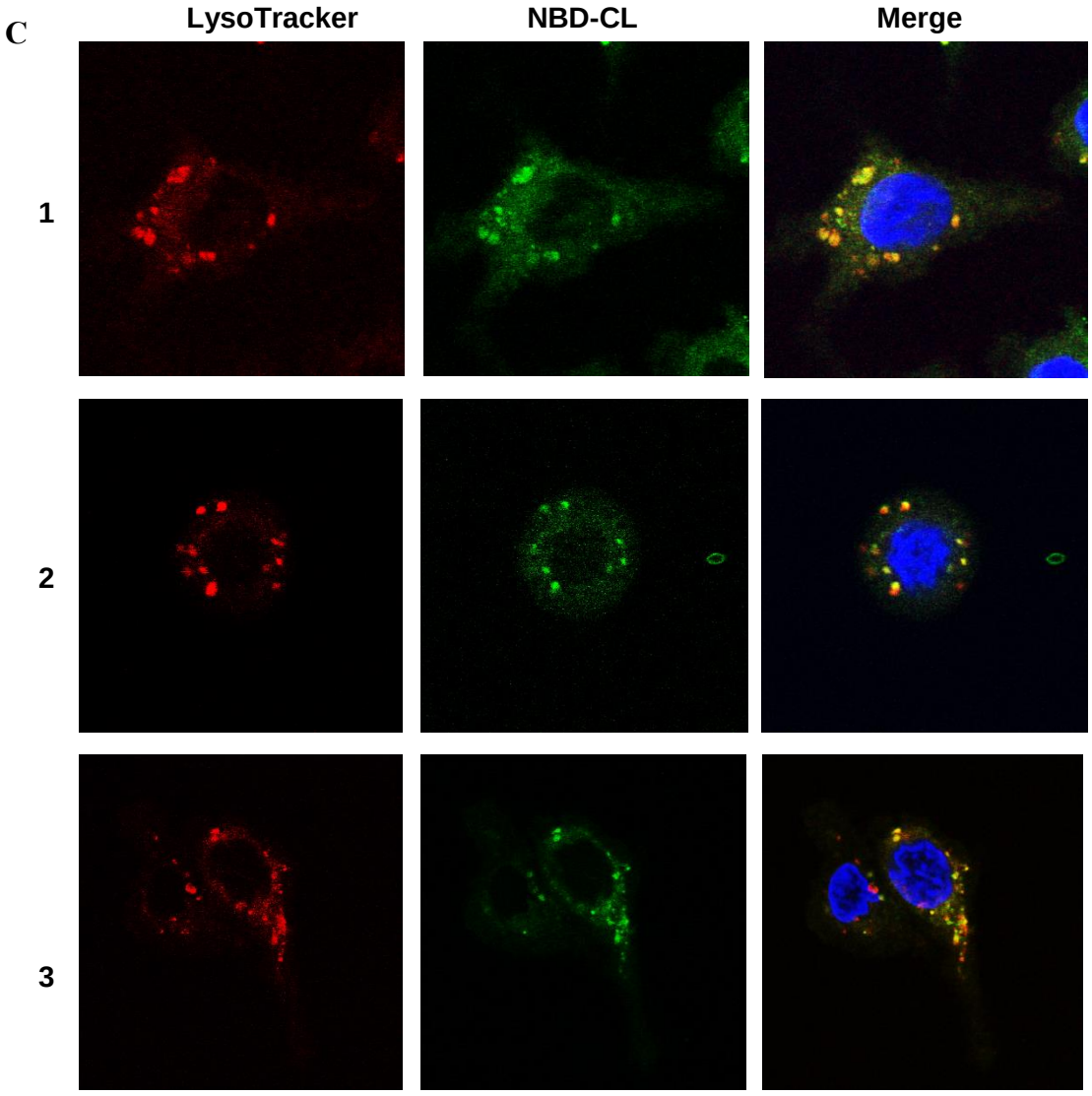
C
LysoTracker
NBD-CL
Merge
1
2
3

Fig. S2. CL-expressing liposomes are colocalized with lysosomes in RAW 264.7 cells and primary human macrophages. RAW 264.7 cells were incubated with NBD-labeled CL-liposomes (green, A) or NBD-labeled PC-liposomes (green, B) for 20 min before being incubated with ER-tracker blue-white (blue) and Lysotracker (red). Images were obtained with a Nikon TI inverted microscope equipped with a swept-field confocal head. 3D stack images were deconvolved with the 3D Landweber deconvolution capabilities of Nikon Elements. Images are representative of three experiments. (**C**) HMDMs were incubated with NBD-labeled CL-liposomes (green) before being incubated with non-fluorescent liposomes to remove nonspecific binding. The cells were then incubated with LysoTracker-Red-DND-99 (LysoTracker, red) and DAPI (blue) to stain nuclei. Images were captured with a confocal microscope. Three representative single-plane images are shown.

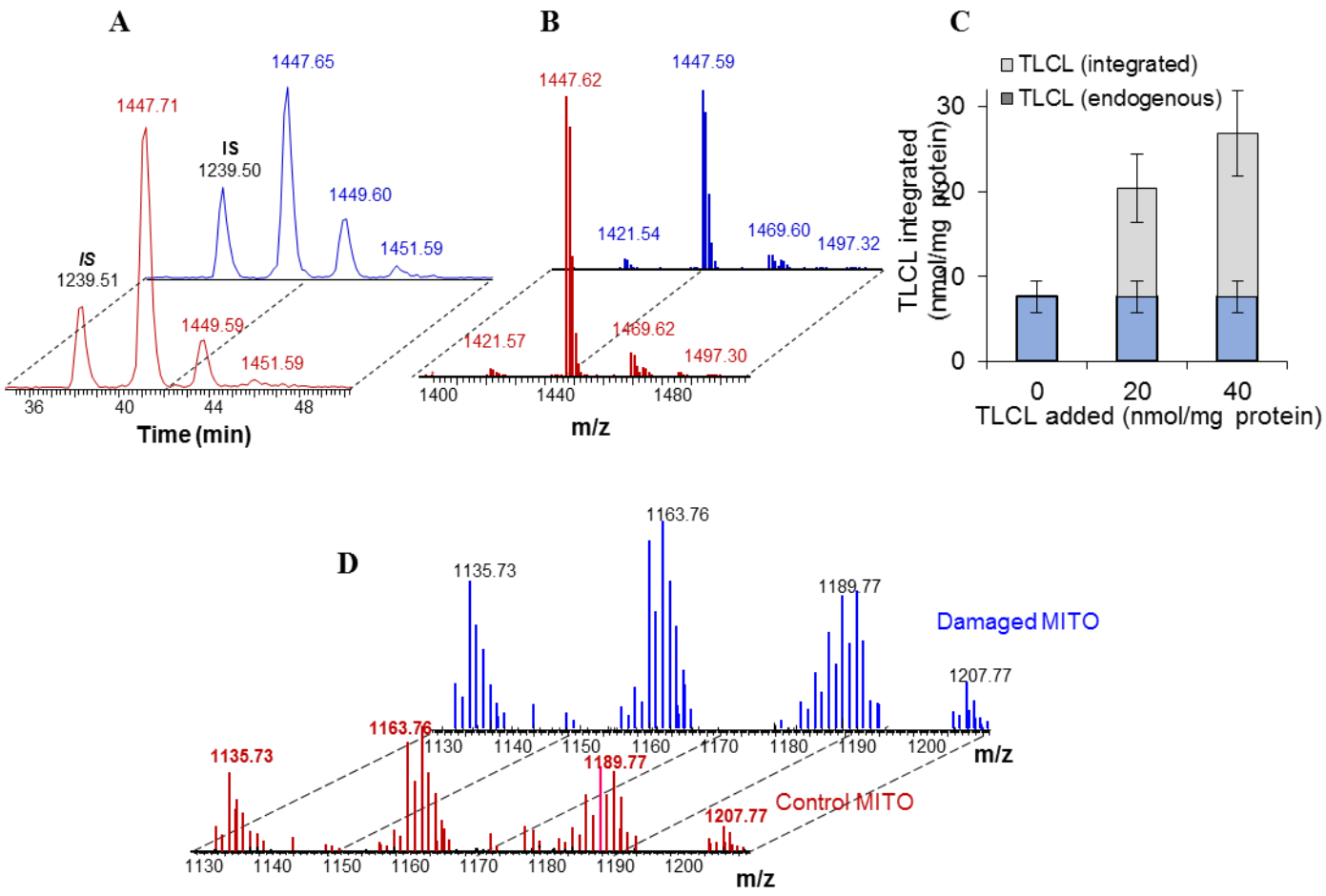

Fig. S3. Integration of exogenous TLCL and the analysis of externalized CL on mitochondria. (**A** to **C**) Mouse liver mitochondria were incubated for 40 min at 22°C in the absence (blue) or presence (red) of TLCL, washed to remove unintegrated TLCL, and then subjected to LC-MS analysis to determine integration efficiency. (A) Typical LC-MS base profiles. (B) Full MS spectra. IS, internal standard. (C) Relative amounts of endogenous TLCL (blue) and integrated exogenous CL (gray) after the incubation of mitochondria with 0, 20, or 40 nmol of TLCL/mg mitochondrial protein. Data are means ± SD of three experiments. *$P < 0.05$ by t-test. (**D**) Control (red) and damaged (blue) mitochondria isolated from MEFs were incubated with phospholipase A_2 and then subjected to the extraction of lipids, which were analyzed by LC-MS to detect mono-lysoCL, a product of the action of phospholipase A_2 on externalized CL. Spectra show a two-fold increase in externalized CLs in damaged mitochondria versus untreated controls for the indicated species. Data are representative of three independent analyses.

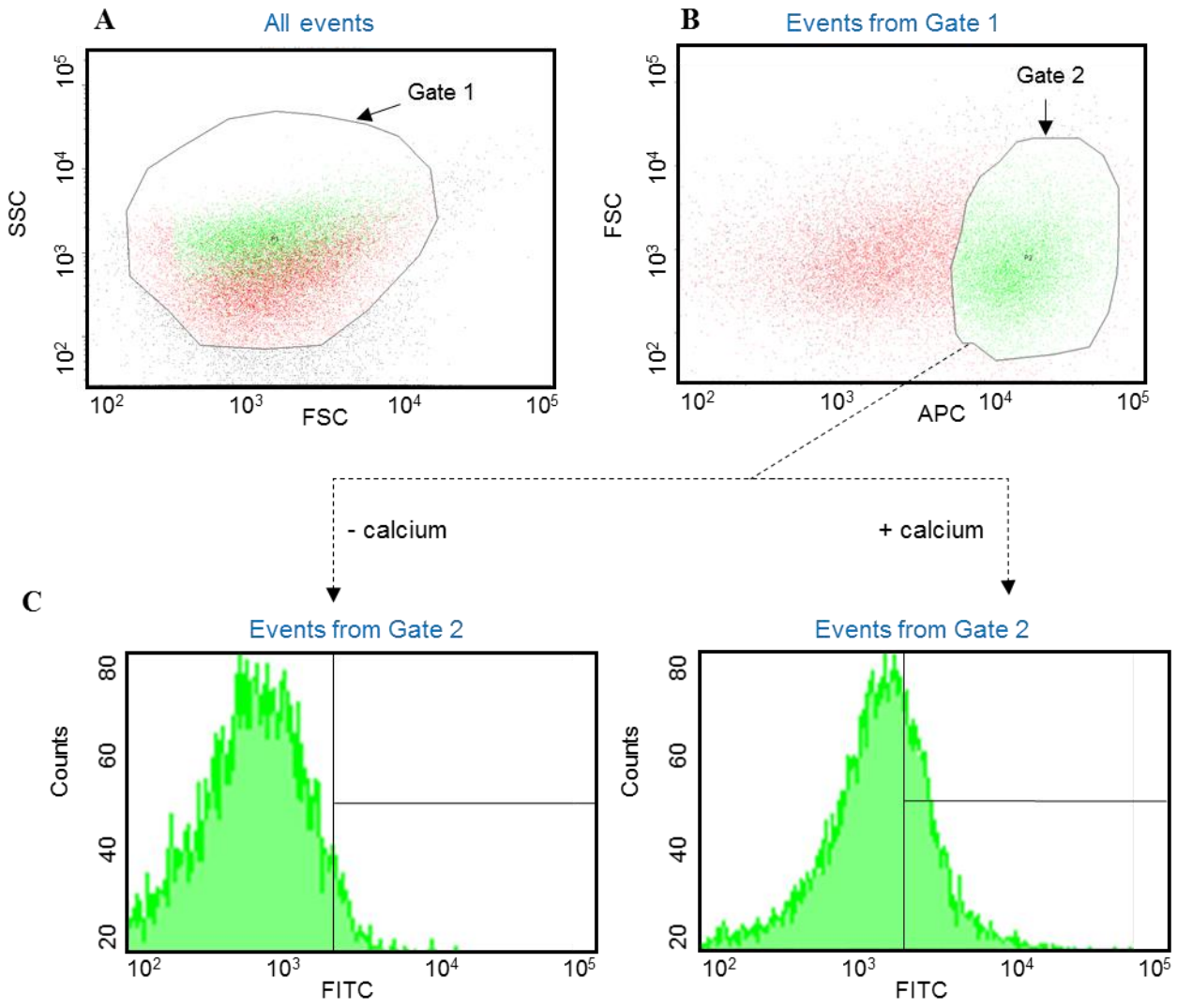

Fig. S4. Gating strategy for the staining of mitochondria with FITC-conjugated annexin V. (**A** to **C**) Assessment of the binding of annexin V–FITC to mitochondria isolated from MEFs was performed with a flow cytometer. Mitotracker Red (PE)–labelled mitochondria were gated (A, Gate 1) based on forward scatter (FSC) and side scatter (SSC). A region having moderate to high PE fluorescence was then selected (B, Gate 2) to assess the Ca^{2+}-dependent binding of annexin V–FITC (C). All assessments of the binding of annexin V to mitochondrial suspensions were performed in the absence and presence of 200 μM Ca^{2+} to rule out signals resulting from nonspecific binding events.

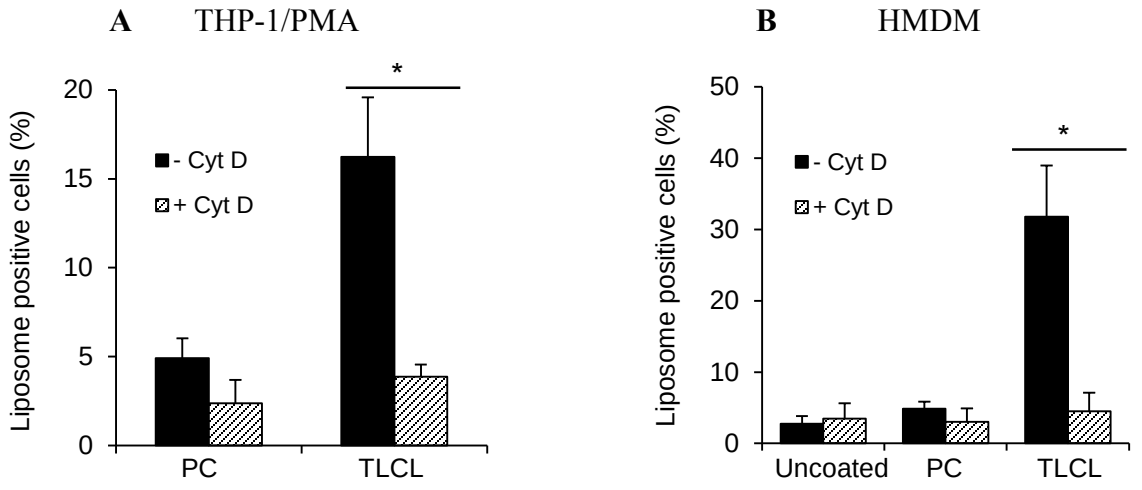

Fig. S5. Phagocytosis of mitochondria presenting TLCL on their surface. (**A** and **B**) PMA-differentiated THP-1 cells (A) and human MDMs (B) were left untreated or were pretreated with 20 μM cytochalasin D (CytD) before being incubated with Mitotracker Red–labeled mitochondria that were uncoated or presented either TLCL (CL) or DOPC on their surface. The cells were then washed and trypsinized and the extent of their phagocytosis of the mitochondria was assessed by flow cytometric analysis. Data are means ± SD of three to five experiments. **P* < 0.05 by t-test.

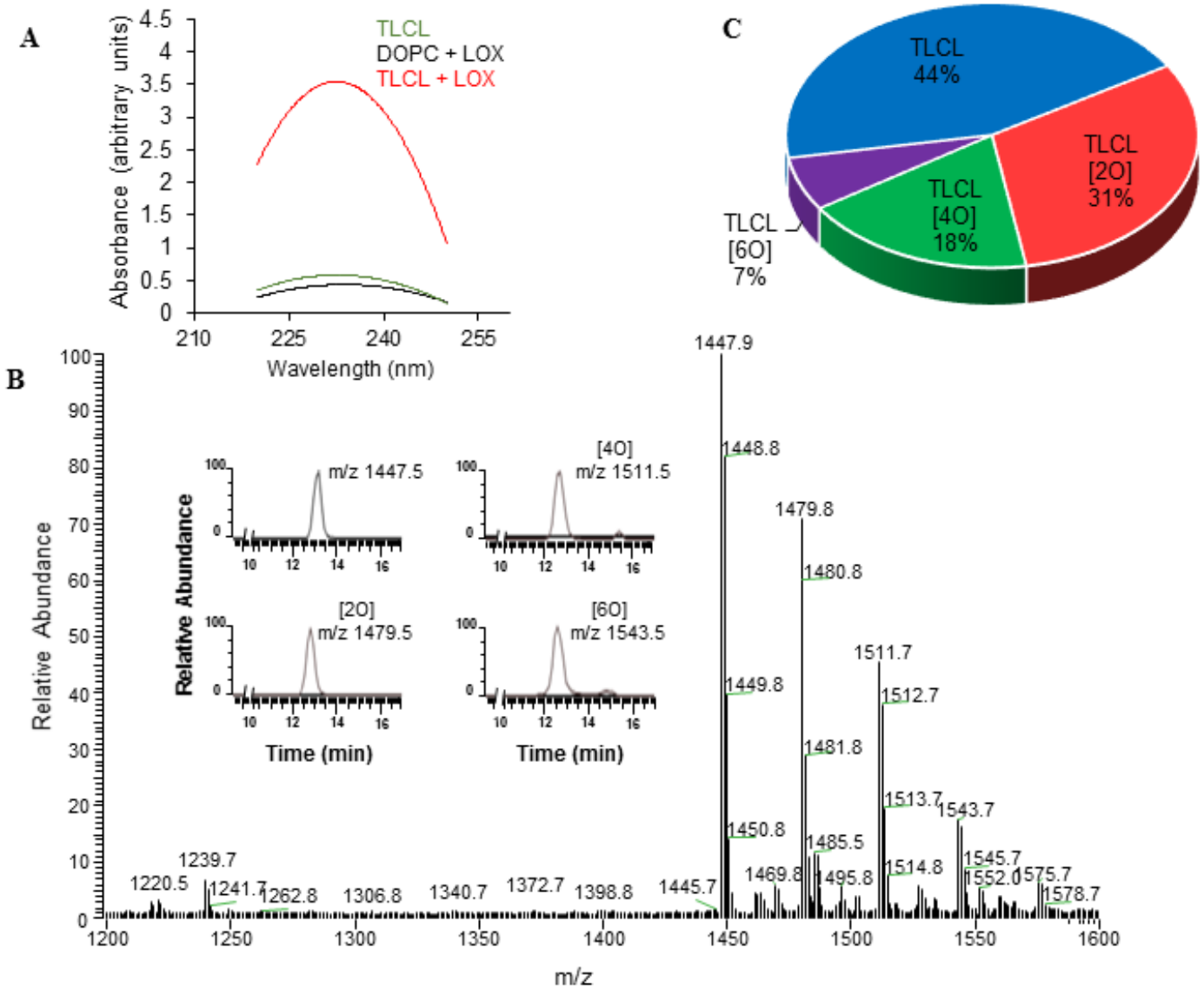

Fig. S6. Oxidation of TLCL-liposomes by soybean LOX. (**A** to **C**) LUVs composed of DOPC or TLCL in DOPC were incubated for 16 hours at 37°C in the presence or absence of soybean lipoxygenase (LOX, 2000 U/mg phospholipid). (A) Lipid peroxidation was established by measuring the absorption of the samples at 235 nm. (B and C) Lipid peroxidation was confirmed by LC-MS analysis of the lipid extracts. (B) Inset: Plots show the relative abundances of the oxidized TLCL molecular species. (C) The relative abundances of the different molecular species of oxidized TLCL. The numbers of oxygen atoms in each identified molecular species of TLCL are denoted within brackets. Data are representative of three experiments.

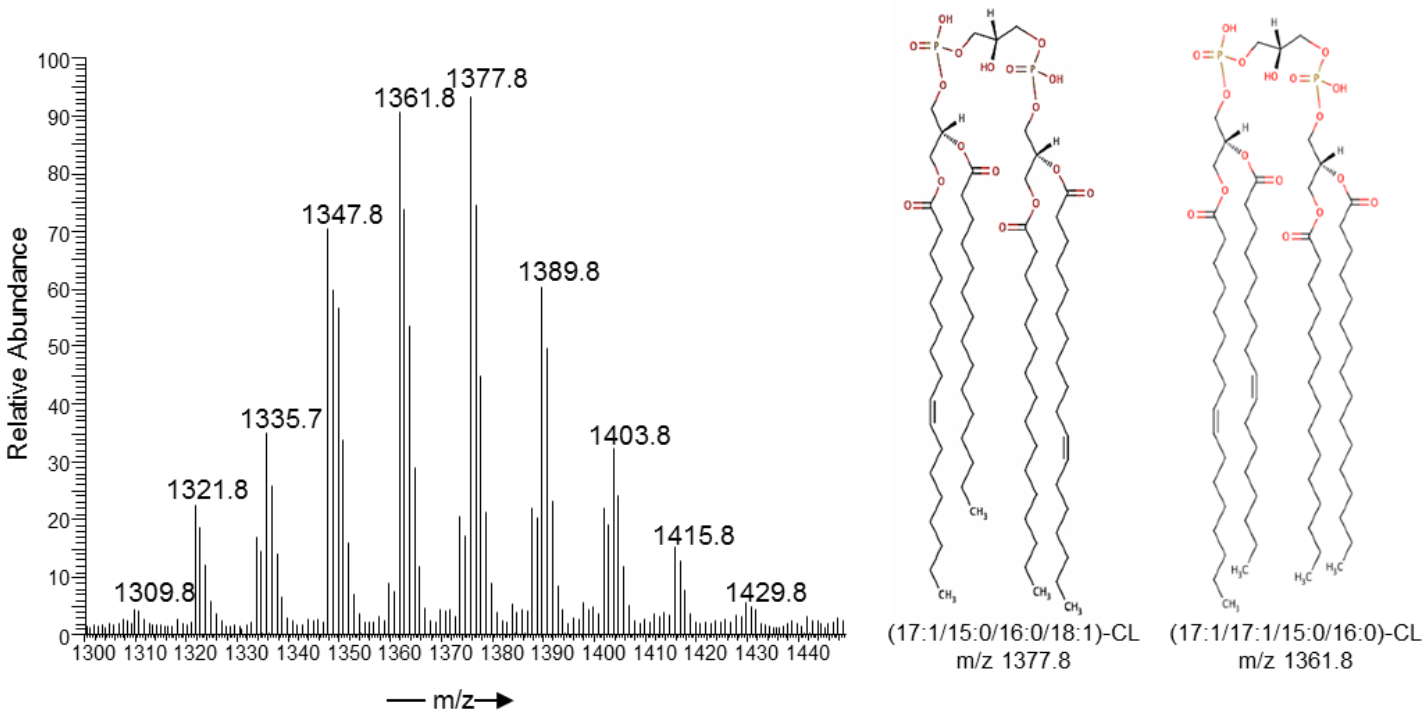

Fig. S7. LC-MS analysis of the different molecular species of CL in *E. coli*. Left: Purified CL derived from *E. coli* was analyzed by LC-MS to determine the relative abundances of each molecular species of CL. Right: The 2D structures of the two most abundant species of CL: 17:1/15:0/16:0/18:1-CL (m/z = 1377.8) and 17:1/17:1/15:0/16:0-CL (m/z = 1361.8).

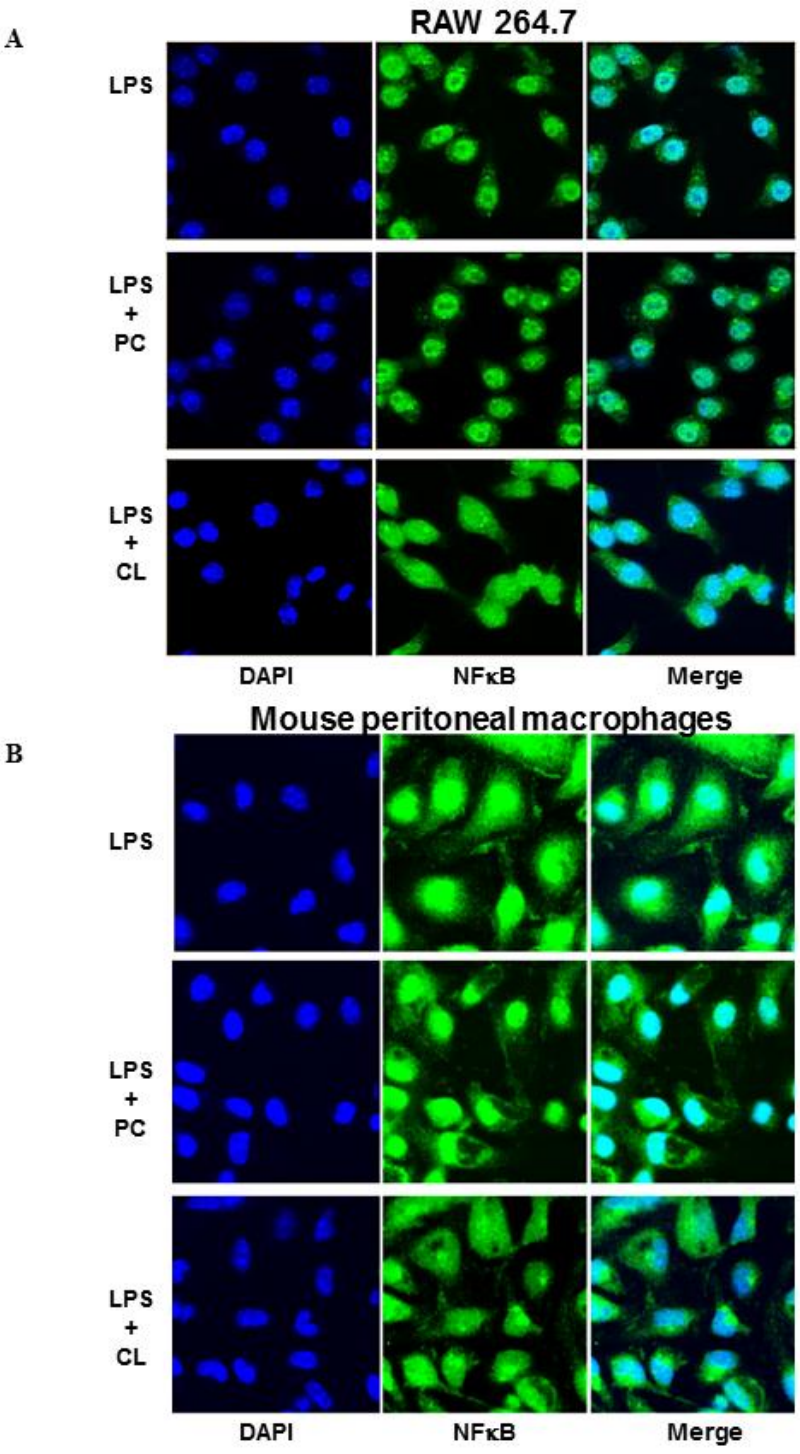

Fig. S8. CL inhibits the nuclear translocation of NF-κB. (**A** and **B**) RAW 264.7 cells (A) and MPMs (B) were incubated for 60 min with LPS alone or in the presence of liposomes composed of PC or TLCL (11.4 nmol CL). The cells were fixed with PFA, permeablized, stained for NF-κB, and counterstained with DAPI. Confocal projection images are representative of three experiments.

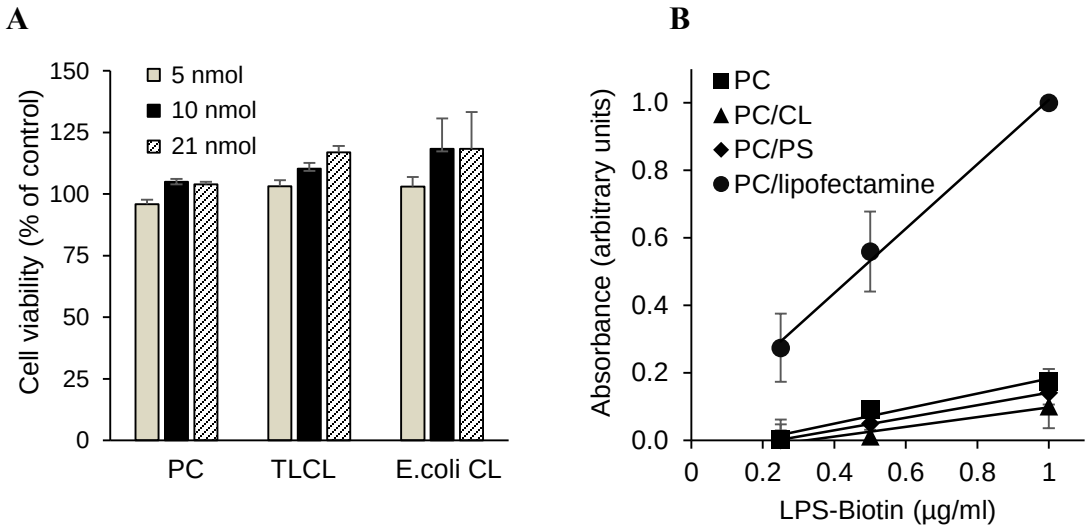

Fig. S9. Inhibition of the LPS-dependent production of cytokines is not a result of a loss in cell viability or the blocking of LPS by CL-liposomes. (**A**) RAW 264.7 cells (100,000 cells) were incubated for 16 hours with LPS (100 ng/ml) and the indicated amounts of PC-, TLCL-, or *E. coli* CL–liposomes. Cell viability was then assessed with Alamar blue. The numbers of viable treated cells are expressed as a percentage of the number of viable untreated control cells. The CL:cell ratio used in the cytokine-retrieval experiments (Fig. 5) corresponds to 10 nmol/100,000 cells. Data are means ± SD of three experiments. (**B**) Liposomes (38 nmol total lipid) composed of the PC alone or TLCL (CL), PS, or lipofectamine in PC (base lipid) were immobilized overnight on ELISA plates. After blocking with 0.5% ovalbumin, the plates were incubated for 60 min with serial dilutions of biotinylated LPS. The binding of LPS to the plates was visualized with HRP-conjugated streptavidin. Cationic liposomes composed of lipofectamine in PC (the base lipid) were used as a positive control to demonstrate the validity of the binding assay. Data are means ± SD of three experiments.

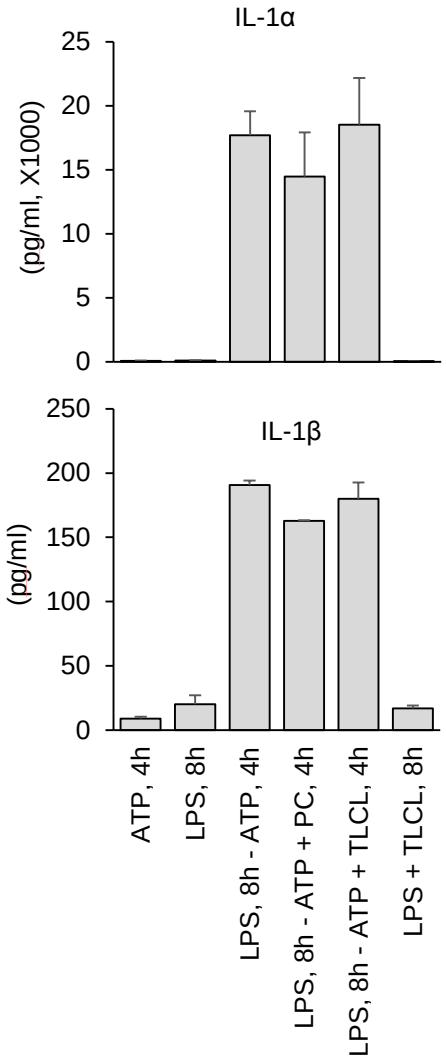

Fig. S10. **CL does not inhibit ATP-induced inflammasome activation in LPS-primed cells.** MPMs from WT mice were pretreated (primed) with LPS for 8 hours before being subjected to a subsequent 4-hour incubation with the indicated reagents (ATP and different liposomes). As negative controls, cells were treated with either ATP or LPS alone. Cell culture medium was then analyzed by Luminex assay to determine the amounts of secreted IL-1α (top) and IL-1β (bottom). Data are means ± SD of three experiments.

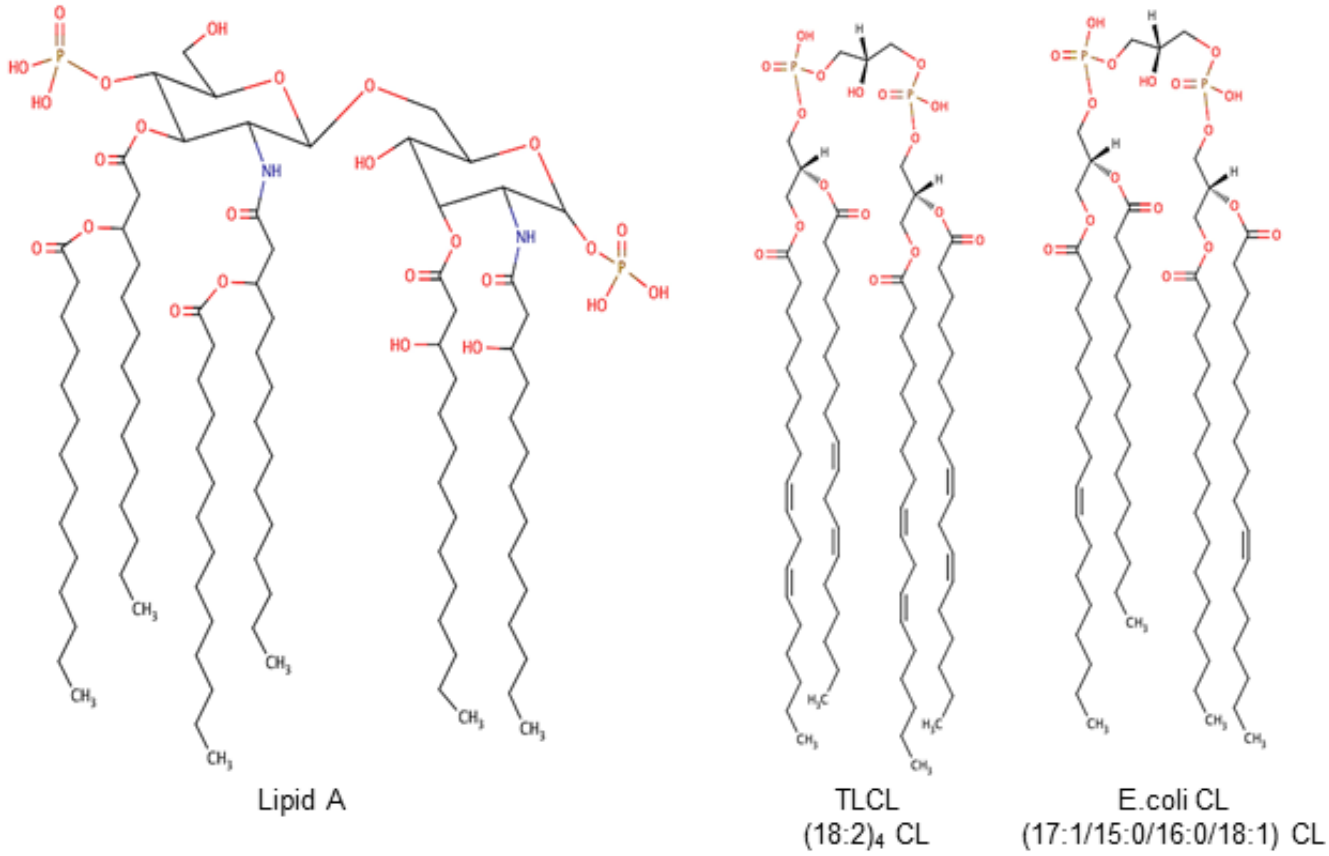

Fig. S11. The 2D structural representations of lipid A, TLCL, and *E. coli* CL.

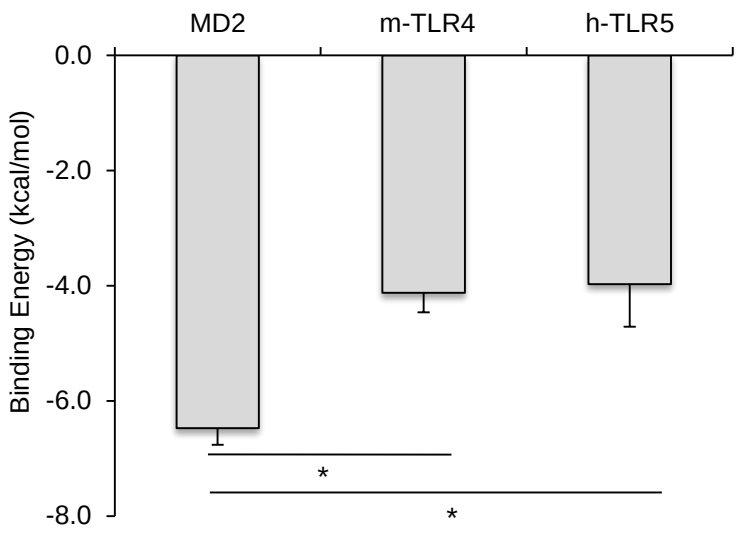

Fig. S12. Comparison of the binding affinities of TLCL for MD2, TLR4, and TLR5. TLCL was docked to the crystal structure of MD2, mTLR4, and hTLR5 with the AutoDock Vina program (http://vina.scripps.edu). The structure of full-length mTLR5 was unavailable. Binding energies obtained from this analysis revealed that the binding affinity of TLCL for MD2 is substantially greater than that for TLR4 and TLR5 based on one-way ANOVA analysis with Bonferroni correction. *$P < 0.05$.

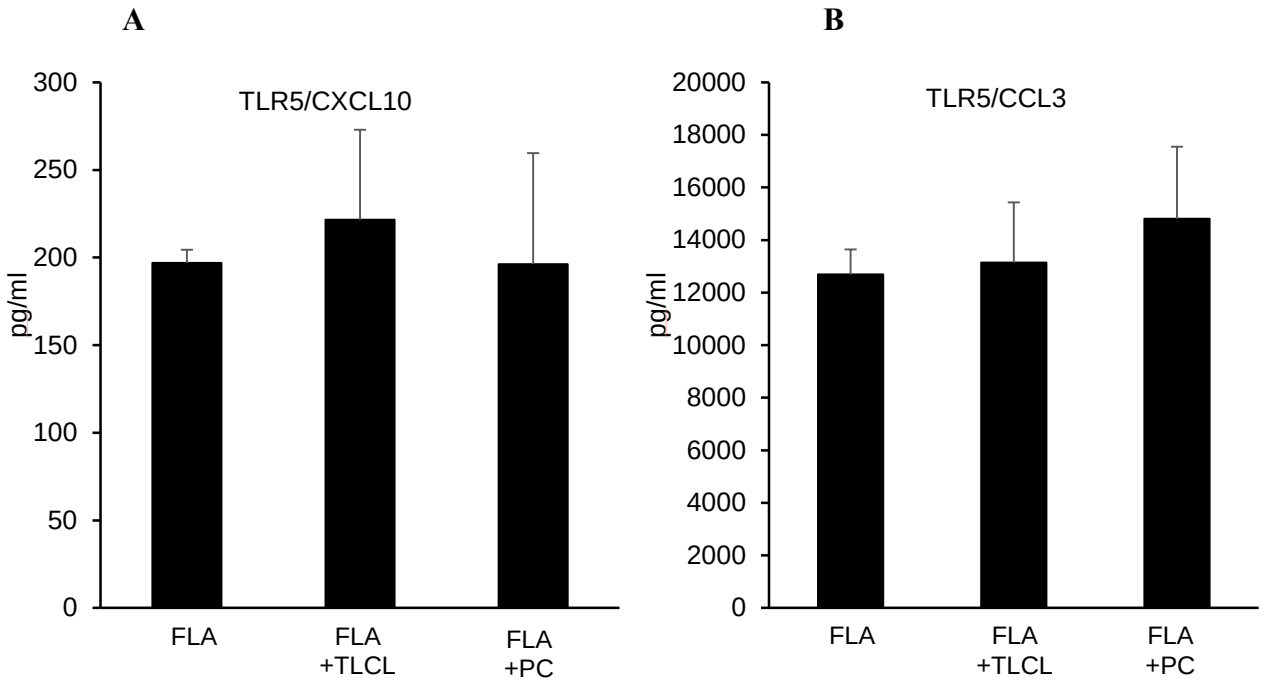

Fig. S13. CL does not inhibit the flagellin-stimulated secretion of cytokines. RAW 264.7 cells were incubated for 16 hours with the TLR5 ligand flagellin (FLA) in the absence or presence of TLCL-liposomes or PC-liposomes. Cell culture medium was then analyzed by Luminex assay to determine the concentrations of CXCL10 and CCL3. Data are means ± SD of three experiments.

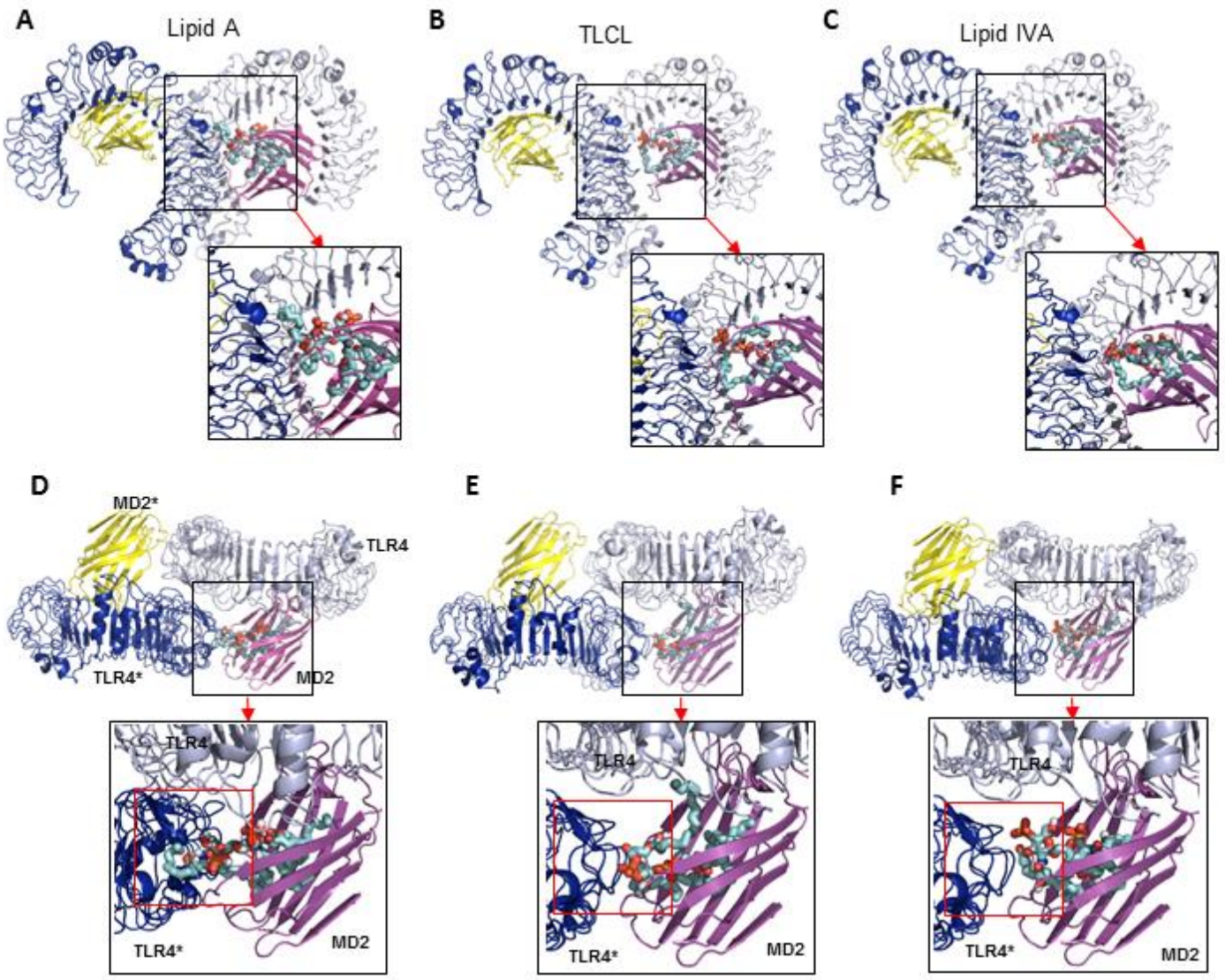

Fig. S14. Predicted binding poses of lipid A, TLCL, and lipid IVA to the TLR4-MD2 complex as determined by molecular docking simulations. (**A** to **F**) Top-view (A to C) and side-view (D to F) images of the top-ranked models for the binding of lipid A, TLCL, and lipid IVA to murine TLR4-MD2. Insets: magnified views of the boxed regions. MD2 and MD2* are in magenta and yellow; whereas TLR4 and TLR4* are in gray and blue. For the lipids, acyl chains are in cyan, nitrogen is in blue, oxygen is in red, and phosphorous is in orange.

Table S1. The binding energies of lipid A, TLCL, and *E. coli* CLs with MD2. Lipid A, TLCL, and *E. coli* CLs were docked onto the crystal structure of MD2 with the AutoDock Vina program. Binding energies were then determined for the lowest energy conformations obtained with this program.

Lipids	Lipid A	TLCL	*E. coli* CL 17:1/15:0/16:0/18:1	*E. coli* CL 17:1/17:1/15:0/16:0
Binding Energy (kcal/mol)	-6.5 ± 0.2	-6.5 ± 0.3	-6.3 ± 0.3	-6.3 ± 0.2